Population Balance Modeling of Particle Size Distribution in Monomer-Starved Semibatch Emulsion Polymerization

Shahriar Sajjadi
Div. of Engineering, ECLAT, King's College London, London WC2R 2LS, U.K.

DOI 10.1002/aic.11917
Published online August 4, 2009 in Wiley InterScience (www.interscience.wiley.com).

The evolution of particle size distribution (PSD) in the monomer-starved semibatch emulsion polymerization of styrene with a neat monomer feed is investigated using a population balance model. The system under study ranges from conventional batch emulsion to semicontinuous (micro)emulsion polymerization depending on the rate of monomer addition. It is shown that, contrary to what is often believed, the broadness of PSD is not necessarily associated with the length of nucleation period. The PSDs at the end of nucleation are found to be independent of surfactant concentration. Simulation results indicate that at the completion of nucleation the particle size is reduced and the PSD narrows with decreasing rate of monomer addition despite nucleation time increasing. The broad distribution of particles frequently encountered in semibatch emulsion polymerizations is therefore attributed to stochastic broadening during the growth stage. The zero-one-two-three model developed in this article allows perceiving that the dominant kinetic mechanism may be different for particles with different sizes. © 2009 American Institute of Chemical Engineers *AIChE J*, 55: 3191–3205, 2009

Keywords: particle nucleation, emulsion polymerization, microemulsion polymerization, micelles, modeling, semibatch reactors

Introduction

Monomer-starved semibatch or semicontinuous emulsion polymerization is a unique process in which ultrafine particles, usually obtained from microemulsion polymerization, can be produced. This process, however, has a significant advantage over microemulsion polymerization which uses a high concentration of surfactant and is limited to rather low solids content. The enhanced particle formation via polymerization with a low concentration of monomer was first reported by Harada and Nomura,[1] and Chatterjee et al.[2] The monomer distribution ratio between the initial reactor charge and the feed, and the rate of monomer addition play important roles in the kinetics of particle formation in the semibatch emulsion polymerization.[3] In practice, most semibatch emulsion polymerization reactors start with 10–20% of the total monomer in the recipe as the initial monomer charge. Particle nucleation stage in such processes usually occurs under flooded conditions according to the conventional emulsion polymerization. To control the molecular weight, copolymer composition, or rate of polymerization, however, the growth stage is usually carried out under monomer-starved conditions. Based on such start up, it is not surprising that some investigators found no significant change in the particle size distribution (PSD) of latexes from batch and semibatch polymerization reactors.[4] It has been recently shown that if the particle formation in a semibatch polymerization reactor is conducted under monomer-starved conditions, a large number of small particles can be produced.[5,6] It appears that this has been a missing opportunity for the latex industry to use starved nucleation to tailor make particles with desired size average and size distribution.

Correspondence concerning this article should be addressed to S. Sajjadi at shahriar.sajjadi-emami@kcl.ac.uk.

In a fully monomer-starved semibatch emulsion process, polymerization starts with an aqueous solution containing a surfactant and an initiator (micellar solution), and then the whole monomer is added to the solution over the time. The starting micellar solution may be considered similar to a microemulsion. For the same reason some investigators have chosen terms associated with microemulsion, such as semibatch micoemulsion polymerization, to address this process.[7–11] It has been shown that for the styrenic type monomers under starved conditions, number of particles (N_p) varies with the rate of monomer addition (R_a) according to $N_p \propto R_a^{-2/3}$; a lower rate of monomer addition results in smaller particles.[12] The breadth of PSD in a monomer-starved semibatch emulsion polymerization can also be altered by variation in the rate of monomer addition. PSD of emulsion latexes, in addition to the average size of particles, has significant implications in properties such as latex rheology, film formation, adhesion, etc. It was shown experimentally,[3] and then confirmed by simulation,[13] that the PSD of particles formed in the semibatch emulsion polymerization with a neat monomer feed depicts a shoulder on the smaller size range when nucleation starts under flooded conditions and then continues into starved conditions. This condition may occur when the rate of monomer addition is sufficiently high to allow polymerization to start under flooded conditions, but not too high to prevent extension to starved conditions.

PSD of latexes are often correlated with the length of nucleation time. A short nucleation time in the conventional batch emulsion polymerization delivers a sharp distribution, whereas a long nucleation time is usually associated with a broad size distribution. In line with above, it came as no surprise that the PSDs of the latexes made by monomer-starved semibatch emulsion polymerizations with a neat monomer feed were found to be broader than those from the conventional batch emulsion polymerization.[14] However, recent experimental results clearly indicate sharp PSDs for latexes from semibatch emulsion polymerization.[15,16] In this article, we aim to elucidate this controversy by developing a theoretical population balance model for the evolution of the PSD in the monomer-starved semibatch emulsion polymerization of styrene. The system of interest consists of two stages: (1) Polymerization starts with monomer-swollen micelles with no monomer droplets present, and particle formation occurs under fully monomer-starved conditions via addition of a neat monomer feed. The end of nucleation is marked by depletion of emulsifier micelles. This part is similar to a semibatch microemulsion polymerization. (2) Particle growth continues under monomer starved conditions with further addition of monomer. No PSD modeling has been reported for this system so far.

PSD Model Development

Min and Ray[17] pioneered modeling of PSD in emulsion polymerization. Their comprehensive model was presented by taking into account two major events including particle formation by micellar and homogenous nucleation mechanisms and particle growth by polymerization and coagulation mechanisms. Some other models, mostly similar in principles, have been proposed by some other investigators for different purposes such as new reactor types, control, and optimization of PSD as well as molecular weigh distribution.[13,18–23] These models have been recently reviewed.[24] Generally, the PSD models can be classified under two headings: zero-one and pseudo-bulk kinetics models. Zero-one models apply to cases in which particles cannot contain more than one growing radical; the average radical number per particle is significantly smaller than one ($\bar{n} << 0.5$). In a zero-one system, the entry of a radical into a latex particle, which already contains a growing radical, results in an instantaneous termination. Whereas pseudo-bulk model applies to the cases where particles undergo a uniform growth, via containing a large number of growing radicals ($\bar{n} >> 0.5$).

Zero-one model is usually applicable to small particles for which the rate of radical loss is high due to rapid radical desorption to the aqueous phase or termination in the particles. Pseudo-bulk models are applicable to large and viscous particles. The latter is usually achieved in high-conversion polymerizations. The high viscosity attained in the particles hinders termination and allow particles to accommodate several radicals. Particles formed in the monomer-starved semibatch emulsion polymerizations of monomers with a high T_g, such as styrene, can be subscribed to both models as they are usually small and highly viscous. The formation of a large number of polymer particles in the monomer-starved emulsion polymerization, however, may significantly shifts the kinetic regime of polymerization so that most particles become restricted to either zero or one radical.[25] Despite this, the presence of particles containing a few radicals in the overall population of particles can not be ignored. Although the effect may not be significant in terms of reaction rate, it can lead to significant variations in the PSDs.[26] The application of pseudo-bulk model is justified only if $\bar{n} >> 0.5$. For monomer-starved nucleation with a small $\bar{n}$, a full account of compartmentalization can be taken into consideration by assuming a zero-one-two or zero-one-two-three system. In the subsequent section, we show that such assumption is sufficient to address multiradical particles in monomer-starved semibatch emulsion polymerization processes.

For calculation of PSD of latexes, it is essential that the variation of all kinetic parameters with particle size and monomer concentration to be considered. The model features are described as follows.

Polymer particles population balances

The rate of particle formation is the sum of particle formation by homogeneous and micellar nucleations.

$$\frac{\partial N_p}{\partial t} = k_{pw}^{j_{cr}-1}[I\dot{M}_{j_{cr}-1}][M]_w + \rho_{micelle}N_m \quad (1)$$

where $[M]_w$ is the monomer concentration in the water phase, $[I\dot{M}_{j_{cr}-1}]$ is the concentration of initiator-derived radicals with chain length $j_{cr}-1$, $k_{pw}^{j_{cr}-1}$ is the propagation rate constant of radicals with the length of $j_{cr}-1$ in water, $\rho_{micelle}$ is the total rate coefficient for entry of initiator-derived radicals into a micelle, and N_m is the micelle concentration. The critical chain length j_{cr} is the length at which the chain precipitates in the water phase to form a precursor particle. The end of nucleation

is marked by the time that all emulsifier micelles are depleted ($N_m = 0$) and variations in the number of particles become negligible. For the styrene emulsion polymerization at the condition of this study, the contribution of homogeneous nucleation to the overall particle formation is not appreciable. However, it was included in the model for the sake of completeness.

A distinction is made between oligoradicals generated from the decomposition of the initiator in the water phase and those formed from desorbed monomeric radicals. Only monomeric radicals can desorb from the polymer particles. Exited hydrophobic monomeric radicals have extremely short relaxation time in the micelles thus their fate is either to re-enter polymer particles or to terminate in the water phase so they do not directly involve in nucleation.[20]

It is assumed that particles can contain up to three free radicals during the growth stage. Entry of a radical into a polymer particle containing three radicals is assumed to lead instantaneously to a termination reaction (i.e., generation of particles with two radicals). In view of the high concentrations of emulsifier, particle coagulation is assumed to be negligible.

Because of a high mobility of radicals formed by radical transfer and the small size of polymer particles formed under starved conditions, it is assumed that the resulting radical undergoes instantaneous termination within the same polymer particle if a growing initiator-derived radical exists. This assumption simplifies the model equations but does not affect the accuracy of the model prediction to a significant extent.

The balance equations for polymer particles with no radical, $n_0(r,t)$, one monomeric radical, $n_1^m(r,t)$, one polymeric radical, $n_1^p(r,t)$, two polymeric radicals, $n_2^p(r,t)$, and three polymeric radicals, $n_3^p(r,t)$, are as follows:

$$\frac{\partial n_0(r,t)}{\partial t} = [\rho(r) + k_{dM}(r)]n_1^m(r) + \rho_{\text{re-entry}}(r)n_1^p(r) + \left[C(r) + 2k_{tr}M_p(r)\right]n_2^p(r) - \rho(r)n_0(r) \quad (2)$$

$$\frac{\partial n_1^m(r,t)}{\partial t} = k_{tr}M_p(r)n_1^p(r) + \rho_{\text{re-entry}}(r)n_0(r) - \left[\rho(r) + k_{dM}(r) + k_p^1 M_p(r)\right]n_1^m(r) \quad (3)$$

$$\frac{\partial n_1^p(r,t)}{\partial t} = \rho_{\text{entry}}(r)n_0(r) + \rho_{\text{re-entry}}(r)n_2^p(r) + \left[3C(r) + 3k_{tr}M_p(r)\right]n_3^p(r) + k_p^1 M_p(r)n_1^m(r) + \delta(r - r_m)\frac{\partial N_p}{\partial t} - k_{tr}M_p(r)n_1^p - \rho(r)n_1^p(r) - \frac{\partial K(r)n_1^p(r)}{\partial r} \quad (4)$$

$$\frac{\partial n_2^p(r,t)}{\partial t} = \rho_{\text{entry}}(r)n_1^p(r) + \rho(r)n_3^p(r) - \left[C(r) + 2k_{tr}M_p(r) + \rho(r)\right]n_2^p(r) - 2\frac{\partial K(r)n_1^p(r)}{\partial r} \quad (5)$$

$$\frac{\partial n_3^p(r,t)}{\partial t} = \rho_{\text{entry}}(r)n_2^p(r) - \left[3C(r) + 3k_{tr}M_p(r) + \rho(r)\right]n_3^p(r) - 3\frac{\partial K(r)n_3^p(r)}{\partial r} \quad (6)$$

where $\rho_{\text{entry}}(r)$ and $\rho_{\text{re-entry}}(r)$ are the total rate coefficient for entry of the initiator-derived and the desorbed radicals into a polymer particle with radius r, respectively, $\rho(r)$ is the total rate coefficient for radical entry into a polymer particle, $C(r)$ is the pseudo-first-order rate coefficient for termination within a particle, $k_{dM}(r)$ is the first-order rate coefficient for desorption of a radical from a polymer particle, k_{tr} is the rate constant for radical transfer to monomer, and $K(r)$ is the propagational growth rate of a particle with radius r containing a growing radical. The last term in Eqs. 4–6, $i\frac{\partial K(r)n_i^p(r)}{\partial r}$, accounts for the rate of loss of particles with size r containing i radicals due to the growth event. $\delta(r - r_m)$ is the delta function, which equals to unity for $r = r_m$ and zero for other values of r, and indicates the radius of particles when they form is equal to the radius of micelles; r_m. For simplicity, all balance equations are written in terms of a liter of water phase.

The overall number of particles with radius r is:

$$n(r) = n_0(r) + n_1^m(r) + n_1^p(r) + n_2^p(r) + n_3^p(r) \quad (7)$$

The total number of polymer particles can be obtained from:

$$N_p = \int_{r_m}^{\infty} n(r)dr \quad (8)$$

Radical balances in the aqueous phase

The oligomeric radicals ($[I\dot{M}_i]$) formed by the initiator decomposition in the water phase can have different fates depending on their chain length: entry into micelles, entry into particles, propagation, and termination in the water phase. It is assumed that only oligomeric radicals with chain length of z and above are sufficiently surface active and thus can enter particles and micelles.[27] Using the steady-state approximation to the rate equations for oligomers up to $i = j_{cr}-1$, we have:

$$[I\dot{M}_1] = \frac{2k_d[I]}{k_{pw}^1[M]_w + k_{tw}[\dot{R}]} \quad (9)$$

$$[I\dot{M}_i] = \frac{k_{pw}^{i-1}[I\dot{M}_{i-1}][M]_w}{k_{pw}^i[M]_w + k_{tw}[\dot{R}]} \qquad i = 2, \ldots z-1 \quad (10)$$

$$\left[I\dot{M}_i\right] = \frac{k_{pw}^{i-1}[I\dot{M}_{i-1}][M]_w}{k_{pw}^i[M]_w + k_{tw}[\dot{R}] + \int_{r_m}^{\infty} k_{ap}^i(r)n(r)dr + k_{am}^i N_m} \qquad i = z, \ldots j_{cr} - 1 \quad (11)$$

where k_{pw}^i is the propagation rate constant of radicals with the length of i in water and $[I]$ is the initiator concentration in the water phase. The rate coefficient of radical propagation in the water phase was assumed to vary with degree of polymerization.[28]

The total aqueous phase radical concentration is

$$[\dot{R}] = \sum_{i=1}^{j_{cr}-1} [I\dot{M}_i] + [\dot{E}] \tag{12}$$

The rate equation for exited radicals into the water phase is

$$\frac{d[\dot{E}]}{dt} = \int_{r_m}^{\infty} k_{dM}(r) n_1^m(r) dr - \int_{r_m}^{\infty} \rho_{\text{re-entry}}(r) n(r) dr - k_{tw}[\dot{E}][\dot{R}] \tag{13}$$

Rate coefficients for radical entry and desorption

Hansen and Uglestad[29] suggested that the absorption efficiency of radicals is a function of their partitioning between particles and water. The growth of the aqueous phase free radicals to a particular degree of polymerization, z, is the primary condition for free radical entry into either latex particles or monomer-swollen micelles.[27] The total rate coefficient for radical entry into a micelle is given by:

$$\rho_{\text{micelle}} = \sum_{i=z}^{j_{cr}-1} k_{am}^i \left[I\dot{M}_i\right] \tag{14}$$

where k_{am}^i is the rate coefficient for radical entry of length i into a micelle of radius r_m. Diffusional mechanism is assumed to be dominant for the entry of the radicals into polymer particles and micelles, indicating that the entry rate constant varies with the size. k_{am}^i is given by:

$$k_{am}^i = 4\pi r_m N_A D_i \tag{15}$$

where D_i is the diffusion coefficient of radicals with chain length i in the water phase which is simply corrected with the diffusion coefficient of monomer in the water phase, D_w, through $D_i = D_w/i$.

The total rate coefficient for radical entry into a polymer particle with radius r is given by:

$$\rho(r) = \rho_{\text{entry}}(r) + \rho_{\text{re-entry}}(r) \tag{16}$$

where

$$\rho_{\text{entry}}(r) = \sum_{i=z}^{j_{cr}-1} k_{ap}^i(r) \left[I\dot{M}_i\right] \tag{17}$$

$$k_{ap}^i(r) = 4\pi r_s N_A D_i \tag{18}$$

where r_s is the radius of monomer swollen particle given by:

$$r_s = \left(\frac{\rho_m}{\rho_m - [M]_p(r) M_{mw}}\right)^{1/3} r \tag{19}$$

where M_{mw} is the molecular weight of monomer. The total rate coefficient for re-entry of the desorbed radicals into a polymer particle is

$$\rho_{\text{re-entry}}(r) = k_{eE}(r) \left[\dot{E}\right] \tag{20}$$

where k_{eE} is the rate coefficient for re-entry of a desorbed radical to a polymer particle given by:

$$k_{eE} = 4\pi r_s N_A D_w \tag{21}$$

The first-order rate coefficient for desorption of a radical from a polymer particle (k_{dM}) is given by[30,31]:

$$k_{dM}(r) = \frac{3 D_p(r) D_w}{\left(([M]_p(r)/[M]_w) D_p(r) + D_w\right) r_s^2} \tag{22}$$

where $D_p(r)$ is the diffusion coefficient of monomeric radicals in a polymer particle with radius r. The aforementioned equation has been derived using Fick's diffusion law for equilibrium conditions and has been widely used to describe radical desorption in emulsion polymerizations. As polymerization proceeds in the particles under monomer-starved conditions, the particles become glassier and the monomer diffusion becomes very slow. The provision for variation of $D_p(r)$ with conversion is presented in the subsequent section.

Rate of growth of particles with different sizes under starved conditions

The rate of growth of a particle with radius r containing a growing radical can be expressed by the following equation:

$$K(r) = \frac{k_p M_{wm} [M]_p(r)}{4\pi r^2 N_A \rho_p} \tag{23}$$

where k_p is the propagation rate constant in the polymer particles.

Diffusion limitations in polymer particles

One of the important features of monomer-starved semibatch emulsion polymerization systems is that they are operated at rather high conversions (high polymer weight ratio in the particles) so that the termination reactions may become diffusion controlled. This may result in an accumulation of radicals in the polymer particles. The variations in the termination constant with monomer concentration in the particles, and thus with the particle size, are not exactly known for small polystyrene particles. The reduction in the termination rate coefficient in the polymer particles (k_{tp}) at high conversions is estimated by the following empirical relation[32]:

$$k_{tp}(r) = k_{tp0} \exp\left(-19 w_p^{2.1}(r)\right) \tag{24}$$

where $w_p(r)$ is the polymer weight ratio in polymer particles with radius r, and k_{tp0} is the intrinsic termination rate constant. The pseudo-first-order rate coefficient for termination within a particle with radius r, $C(r)$, is defined as:

$$C(r) = \frac{k_{tp}(r)}{N_A v_s(r)} \tag{25}$$

where v_s ($= 4/3\pi r_s^3$) is the volume of monomer-swollen particles.

The rate of propagation often becomes diffusion controlled in the high-conversion regime due to the glass effect. As a

result, the value of k_p will reduce with conversion. The reduction in k_p at high conversions is estimated by the following empirical equation[33,34]:

$$k_p(r) = k_{p0} \quad \text{when} \quad V_f(r) \geq V_{f,cr} \tag{26}$$

$$k_p(r) = k_{p0} \exp\left[-A\left(\frac{1}{V_f(r)} - \frac{1}{V_{f,cr}}\right)\right] \quad \text{when} \quad V_f(r) < V_{f,cr} \tag{27}$$

where k_{p0} is the intrinsic propagation rate constant, V_f(r) is the fractional free volume of a polymer particle with radius r, $V_{f,cr}$ is the V_f at the onset of the glass effect, and A is an adjustable parameter. The fractional free volume of the polymer phase can be calculated by the following equation:

$$V_f(r) = V_{fm}\left(1 - \varphi_p(r)\right) + V_{fp}\varphi_p(r) \tag{28}$$

where $\varphi_p(r)$ is the volume phase ratio of polymer in the polymer particles with radius r, and V_{fm} and V_{fp} are the fractional free volumes of monomer and polymer, respectively. V_{fm} and V_{fp} are calculated as follows:

$$V_{fm} = 0.025 + \alpha_m(T - T_{gm}) \tag{29}$$

$$V_{fp} = 0.025 + \alpha_p(T - T_{gp}) \tag{30}$$

where α_m and α_p are the thermal expansion coefficients of monomer and polymer, respectively. T_{gm} and T_{gp} are the glass transition temperatures of monomer and polymer, respectively.

The decrease in the propagation rate constant at high conversions in fact stems from the reduction in the diffusion coefficient of monomer molecules in the polymer phase. Therefore, the variation of $D_p(r)$ with polymer phase ratio can be easily obtained by:

$$D_p(r) = D_{p0}\frac{k_p}{k_{p0}} \tag{31}$$

where D_{p0} is the intrinsic diffusion coefficient of desorbing monomeric radicals. The rate constant for radical transfer to monomer, k_{tr}, follows the same relative change as k_p under diffusion-controlled conditions; $k_{tr}/k_{tr0} = k_p/k_{p0} = D_p/D_{p0}$, where k_{tr0} is intrinsic k_{tr}. Note that both the gel effect and glass effect are size dependent simply because w_p is different for particles with different sizes.

Monomer partitioning among the polymer phase, micelles, and water phase

We assume equilibrium to be maintained during polymerizations among all phases. In monomer-starved semibatch processes, the average size of particles encountered is usually very small. Morton et al. presented a correlation which dealt with variations in the saturation monomer concentration of latex particles with size. Vanzo et al.[35] extended the Morton's equation to include partial swelling of latex particles under starved conditions:

$$\ln\left(1 - \varphi_p(r)\right) + \varphi_p(r) + \chi\varphi_p^2(r) + \frac{2\bar{V}_m\gamma\varphi_p^{1/3}(r)}{rRT} = \ln\left(\frac{[M]_w}{[M]_{w,sat}}\right) \tag{32}$$

where γ is the interfacial tension, $[M]_{w,sat}$ is the saturation monomer concentration in the water phase, χ is the interaction parameter between the monomer and its polymer, and $\bar{V}_m$ is the molar volume of the monomer.

The monomer concentration in the micelles, $[M]_m$ (in terms of unit volume of the aqueous phase) is proportional to the monomer concentration in the water phase according to the following equation[25]:

$$[M]_m = K_{eq}[M]_w N_m / N_A \tag{33}$$

where K_{eq} is a constant. The number of molecules of styrene solubilized in a micelle, X_M, can be easily obtained from $X_M = [M]_m N_A/N_m$. As X_M decreases with $[M]_w$ in the course of polymerization, the micelles shrink and as a result, some emulsifier molecules are released into the water phase and form new micelles. The size variation of micelles is conformed to a constant surface coverage ratio of emulsifier molecules. An increase in the aggregation number of micelles with $[M]_w$ is given by[25,26]:

$$\Delta n_{agg} = 2K_{eq}[M]_w\frac{V_M}{V_S} \tag{34}$$

where V_S and V_M are the hydrophobic volumes of the surfactant tail and monomer, respectively. The overall aggregation number of a monomer-swollen micelle (n_{agg}) is

$$n_{agg} = n_{agg0} + \Delta n_{agg} \tag{35}$$

where n_{agg0} is the aggregation number in the nonswollen state. From n_{agg} and X_M it is possible to estimate the variation of the volume of a micelle, and thus its radius r_m, in the course of nucleation. The volume of a micelle is the sum of contributions from the hydrophobic volumes of the surfactant tail and monomer from which the radius of micelles can be easily obtained as:

$$r_m = \left(3(n_{agg}V_S + X_M V_M)/4\pi\right)^{1/3} \tag{36}$$

The radius of micelles changes from $r_m = 1.95$ nm, when they contain no monomer ($n_{agg} = 80$), to $r_m = 2.75$ nm when they are fully swollen with monomer ($n_{agg} = 176$). The monomer partitioning among the three phases under starved conditions must satisfy the following mass balance equation:

$$\left(\int_{r_w}^{\infty} M_p(r)V_p(r)dr + [M]_w V_m + [M]_m V_w\right)M_{wm} = m_m \tag{37}$$

where m_m is mass of unreacted monomer, and V_w and $V_p(r)$ (= $4/3\pi r_s^3\ n(r)$) are the volumes of water (1 l) and swollen polymer particles with unswollen radius r, respectively. The monomer concentration in the particles with radius r under starved condition is

$$[M]_p(r) = \left(1 - \varphi_p(r)\right)\frac{\rho_m}{M_{wm}} \tag{38}$$

where ρ_p and ρ_m are densities of polymer and monomer, respectively. The volume phase ratio of polymer particles with radius r is related to the weight ratio of polymer in the particles by:

$$w_p(r) = \left(1 + \frac{1 - \varphi_p(r)}{\varphi_p(r)}\frac{\rho_m}{\rho_p}\right)^{-1} \tag{39}$$

Micelle concentration

For a monomer-starved semibatch emulsion polymerization, surfactant partitions among the three sites available: polymer particles, micelles, and water phase. The total surface area of particles is

$$S_p = 4\pi \int_{r_m}^{\infty} n(r) r_s^2 dr \tag{40}$$

Assuming that the surfactant concentration in the water phase stays at the critical micellar concentration (CMC) value, $[S_{cmc}]$, and the polymer particles are fully covered by emulsifier molecules, the concentration of micelles during nucleation is found with the following equation:

$$N_m = \left([S]N_A - S_p/a_s - [S_{cmc}]N_A\right)/n_{agg} \tag{41}$$

where a_s is the adsorption area occupied by a molecule of emulsifier on the surface of polymer particles, and $[S]$ is the concentration of surfactant per unit volume of water.

Material balances

The mass of polymer in the particles at time t can be obtained by summation of the masses of individual particles:

$$m_p = \frac{4}{3}\pi\rho_p \int_{r_s}^{\infty} r^3 n(r) dr \tag{42}$$

The mass of free (unreacted) monomer in the reactor at time t is

$$m_m = R_a t \rho_m + m_0 - m_p \tag{43}$$

where m_0 is the initial mass of monomer in the reactor at $t = 0$. The instantaneous conversion at time t is defined as the weight ratio of the polymer formed in the reactor to the total monomer fed into the reactor by time t:

$$x_i = \frac{m_p}{R_a t \rho_m + m_0} \tag{44}$$

For the sparingly water-soluble styrene under monomer-starved conditions and in the presence of micelles; $x_i \approx w_p$.

The overall conversion is defined as the weight ratio of the polymer in the reactor to the total monomer in the recipe:

$$x_o = \frac{m_p}{m_{total}} \tag{45}$$

where m_{total} is the total mass of monomer in the recipe per liter of the water phase.

The material balance for the initiator is as follows:

$$\frac{d[I]}{dt} = -k_d[I] \tag{46}$$

where k_d is the rate coefficient for the decomposition of the initiator. It is assumed that the rate of initiator decomposition does not vary with monomer concentration in the water phase.

Model implementation

The partial integro-differential equations were transformed into a set of ordinary differential equations by discretizing the domain of particle size into equally spaced bins (finite difference). The resulting differential equations, together with the algebraic equations describing the reaction (Eqs. 1–46), were numerically solved using a Runge–Kutta fifth-order method. The integral terms in the PBE were approximated using a composite Simpson's rule. Sufficient number of bins was considered to cover the whole span of PSDs encountered in the polymerization systems under study. This number was maximum for the monomer-flooded conditions and minimum for the starved ones where the particle growth was limited. The mid point of each bin was considered as representative of the whole bin size. The rate constants and the parameters required for the mathematical modeling are all obtained from the literature and are listed in Table 1. The

Table 1. The Parameters Used for Simulation of Styrene Emulsion Polymerization at 70°C

Parameter	Value	Reference
k_{pw}^1, l mol^{-1} s^{-1}	1300	28
k_{pw}^2, l mol^{-1} s^{-1}	840	28
k_{pw}, l mol^{-1} s^{-1}	480	28
k_{tw}, l mol^{-1} s^{-1}	3×10^9	28
D_w, cm^2 s^{-1}	1.5×10^{-5}	28
D_{p0}, cm^2 s^{-1}	1.5×10^{-5}	28
$[M]_{w,sat}$, mol l^{-1}	5.6×10^{-3}	28
j_{cr}	5	28
k_{tr0}, l mol^{-1} s^{-1}	9.3×10^{-3}	28
k_{p0}, l mol^{-1} s^{-1}	480	28
k_p^1, l mol^{-1} s^{-1}	$4k_{p0}$	28
k_{tp0}, l mol^{-1} s^{-1}	6.8×10^7	33
ρ_m, g cm^{-3}	0.878	28
ρ_p, g cm^{-3}	1.044	28
$V_{f,cr}$	0.033	34
α_m, 1/°C	0.001	34
α_p, 1/°C	4.8×10^{-4}	34
T_{gm}, °C	−88.2	34
T_{gp}, °C	93.5	34
A	1	34
a_s, Å^2	43	28
S_{cmc}, mol l^{-1}	3.9×10^{-3}	28
n_{agg0}	80	26
V_S, nm^3	0.385	26
V_M, nm^3	0.197	26
K_{eq}, mol^{-1}	1.68×10^4	26
r_m, nm	2.50	26
χ	0.43	30
γ, mN m^{-1}	4.5	30
k_d, s^{-1}	2.2×10^{-5}	28

thermodynamic analysis has showed that the critical chain length for entry of styrenic radicals is 2 or 3.[28] We used these two values of z as adjustable parameters. The nucleation and growth stages were modeled using zero-one and zero-one-two-three model, respectively. The zero-one kinetics was accomplished by assuming $C(r) = n_2 = n_3 = 0$. The glass effect was considered for both nucleation and growth stages, when appropriate. To highlight the importance of zero-one-two-three model and for the sake of comparison, the growth stage for some runs was modeled using zero-one kinetics.

The modeling results indicate a good fit with the experimental ones. Nevertheless, the result section starts with the analysis of the nucleation and growth stages, as they are essential for a better understanding of the evolution of PSD in the course of polymerization. The comparison of the predicted and experimental results is presented at the end.

Results and Discussion

Nucleation stage

Traditionally, the PSD of latexes at the end of nucleation is well correlated with the period of particle formation. In conventional batch emulsion polymerizations, a decrease in the emulsifier concentration or an increase in the initiator concentration is expected to reduce the nucleation time and sharpen the PSD. For the same reason, monodisperse seed polymer particles are usually produced at high temperatures, to increase the rate of radical generation, using a low concentration of surfactant. The rate of particle growth in conventional batch emulsion polymerizations is usually treated as a constant. In monomer-starved semibatch processes, the overall rate of growth of particles can be controlled by the rate of monomer addition as:

$$\mu(t) = \frac{R_a}{N_p} \qquad R_p > R_a \tag{47}$$

where R_a is the volumetric rate of monomer addition in $l\ s^{-1}\ l^{-1}$ (aq). In the aforementioned equation, the difference between monomer and polymer densities and the amount of monomer solubilized in the micelles and dissolved in the water phase have been neglected for simplicity. The aforementioned equation predicts a linear relation between the instantaneous rate of particle growth and the rate of monomer addition. Using the aforementioned equation and similar to the treatment of Smith and Ewart, it is possible to show that the nucleation time is given by[25]:

$$t_f = k(a_s[S])\rho_I^{-1/3}R_a^{-2/3} \tag{48}$$

where k is a numerical constant, and ρ_I is the rate of radical entry into micelles and particles ($= \rho_{micelle} + \rho_{entry}$). The following equation is obtained for the final number of polymer particles:

$$N_p = k(a_s[S])\rho_I^{2/3}R_a^{-2/3} \tag{49}$$

We showed previously that similar exponents with those mentioned earlier can be obtained even if a comprehensive model is used.[25] For starved conditions, V_p can be approximated by

$$V_p = R_a t \tag{50}$$

Knowing that the average volume of particles formed at the end of nucleation ($t = t_f$) is given by $v_p = V_p/N_p$, and using Eqs. 48–50, we conclude

$$\begin{aligned} &v_p = R_a/\rho_I \\ &\text{or} \quad d_v = (6/\pi)^{1/3}(R_a/\rho_l)^{1/3} \end{aligned} \tag{51}$$

The aforementioned equation shows an interesting result; the average volume of polymer particles at the end of nucleation is independent of [S] despite N_p is increasing with [S]. For the sake of comparison, note that v_p at the completion of nucleation in the batch polymerization system increases with $[S]^{0.60}$. For starved conditions, the nucleation time and number of polymer particles are proportional to the emulsifier concentration (Eqs. 48 and 49). But the volume growth rate of polymer particles, μ, is inversely proportional to N_p. So as [S] is doubled, for example, the nucleation period lasts twice that long (see Eq. 48), and two times more particles are formed (Eq. 49). However, the overall volume growth rate of particles is reduced by half compensating the effect of prolonged nucleation. This results in the average particle size being independent of [S]. The occurrence of an identical average size at the completion of nucleation for different surfactant concentrations, as predicted by the aforementioned analysis, may seem to be too simplistic, but can be verified by applying the population balance model developed in this article.

Figure 1 shows the PSDs at the end of nucleation for the runs with [S] = 0.02, 0.04, and 0.08 mol l^{-1} at low- and high-entry rates; $z = 2$ and 3. Interestingly, the PSDs of runs with z =2 fall on the same curve indicating that the PSD at the end of nucleation is independent of surfactant concentration. It is worth noting that Figure 1 shows the PSDs of the nonswollen polymer particles. The PSDs of the swollen particles, however, are also similar because R_p is tightly controlled by R_a ($R_p \approx R_a$).[25] The results for $z = 3$ show a small discrepancy between the curves. At this value of z, the entry rate is relatively low. A low rate of radical entry can lead to growing stochastic broadening of the distribution with increasing [S].

The most striking result from Eq. 51 is that the average volume of particles (v_p) at the end of nucleation increases linearly with R_a, if all other variables fixed. The effects of R_a on PSDs are shown in Figure 2. Distinctive PSDs were obtained for the runs using different R_a values. Among the semibatch runs, the run with the highest R_a resulted in the broadest PSD at the end of nucleation. In accordance with Eq. 51, the average volume of particles almost doubled as R_a increased twice ($v_p \propto R_a^{1.0}$). With increasing R_a, eventually a point is reached after which the latex particles become saturated with the monomer and polymerization fully occurs under flooded conditions. Figure 2 shows that the batch operation produced the broadest distribution. The reason for PSD sharpening with decreasing R_a is the reduced rate of

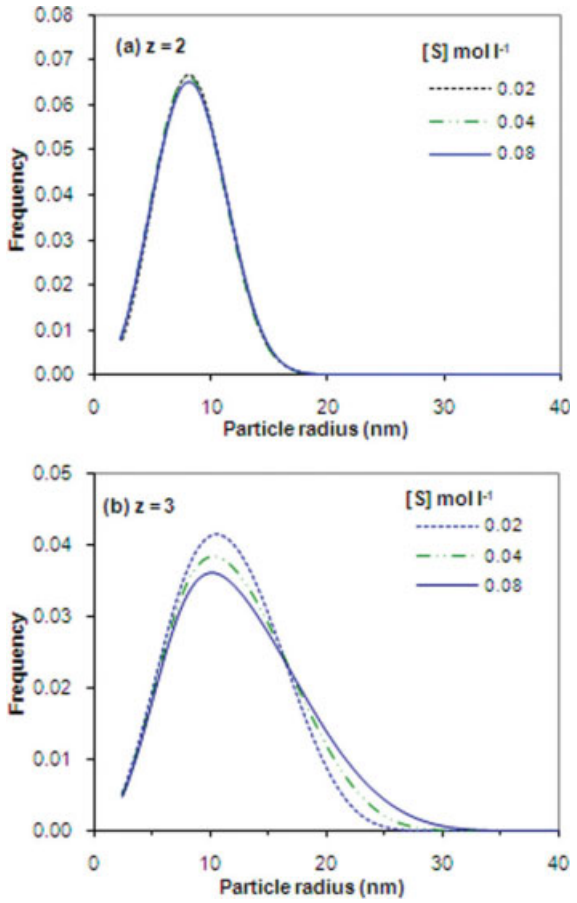

Figure 1. PSDs at the end of nucleation for various surfactant concentrations: (a) High-entry rate; $z = 2$, (b) low-entry late; $z = 3$ ($[I] = 2 \times 10^{-3}$ mol l^{-1}, $R_a = 2.6 \times 10^{-5}$ l s^{-1} l^{-1} (aq).

[Color figure can be viewed in the online issue, which is available at www.interscience.wiley.com.]

growth of particles due to enhanced radical desorption under monomer-starved conditions. Particles formed under starved condition grow to a limited extend during nucleation, as a result their average size is reduced and their size distribution narrows. This will be further discussed in our future publication. It may be concluded that particle nucleation under starved conditions can be used to produce sharp PSDs. This conclusion may seem to be in contrast with the literature that indicate particle nucleation under monomer-starved conditions will lead to the formation of polymer latexes with broad size distributions.[14] We present the reasons for PSD broadening in the next section.

Growth stage

Distribution of Radicals in Particles. For the conventional monomer-starved semibatch emulsion polymerization of styrene most of the reaction lies within interval III during which the movements of macroradicals are hindered by the high viscosity of the reaction medium. Slow propagation and termination rates can lead to an accumulation of radicals in the particles. The model presented here makes it possible to obtain information regarding the number of radicals housed within particles of various sizes at high conversions. Figure 3 shows the model predictions for the population of particles containing different number of radicals (0, 1, 2, and 3) and different type of growing radicals (initiator derived versus monomer derived) at the mid of feeding ($t_{1/2}$) for the semibatch runs with two different feed rates. It is seen from Figure 3a that for the higher R_a used, a fraction of particles contain two radicals with a smaller fraction contain three growing radicals. Particles containing monomeric radical are only a negligible fraction of the total. These particles could not be shown in Figure 3 because of a significant difference in their order of magnitudes in comparison with the other particles. For the lower R_a, most particles either do not contain a radical or contain a sole radical. Only very small fraction of particles contain two radicals (Figure 3b). This occurs despite the fact that radicals live longer due to both propagation and termination reactions being diffusion controlled (the rate of propagation for a radical in polymer particles is $k_p[M]_p$, where both k_p and $[M]_p$ are significantly reduced under monomer starved conditions).

In addition to the rate of monomer addition, the surfactant concentration can also play an important role in the kinetics of semibatch emulsion polymerization reactions. Figure 4 shows the predicted PSDs in terms of radical number at the mid of feeding for two surfactant concentrations. For $[S] = 0.02$ mol l^{-1} there exists an appreciable number of particles with one growing radical, though particles containing no radical are still in majority (Figure 4a). For this case particles containing two and three radicals are also important. It is seen from Figure 4b that for the higher surfactant concentration used, $[S] = 0.08$ mol l^{-1}, most particles contain no radical, and a smaller proportion of particles contain one growing radical. For the latter case, only an extremely small fraction of particles contain two radicals.

The behaviors described earlier do not fit the characteristic feature of conventional high-conversion polymerization of styrene which is manifested by a large radical number per

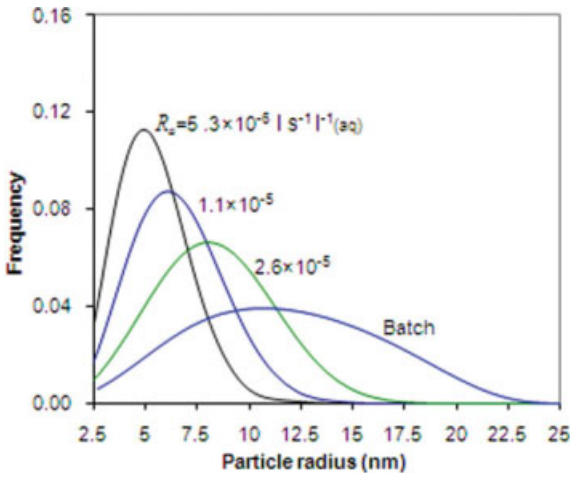

Figure 2. PSDs at the end of nucleation for various rates of monomer addition ($[S] = 0.04$ mol l^{-1}, $[I] = 2 \times 10^{-3}$, mol l^{-1}, $z = 2$).

[Color figure can be viewed in the online issue, which is available at www.interscience.wiley.com.]

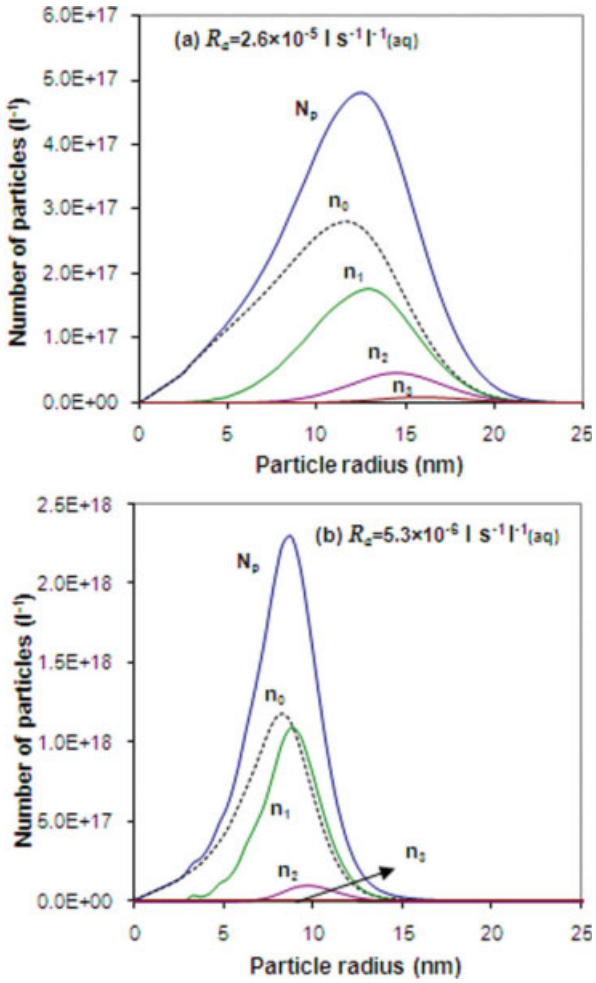

Figure 3. Size distributions for particles containing *n* radicals at the mid of feeding for two rates of monomer addition: (a) 2.6 × 10^{-5} and (b) 5.3 × 10^{-6} l s^{-1} l^{-1} (aq) ([*S*] = 0.04 mol l^{-1}, [*I*] = 2 × 10^{-3} mol l^{-1}, *z* = 2, $t_{1/2}$ = 120 and 240 min for (a) and (b), respectively).

[Color figure can be viewed in the online issue, which is available at www.interscience.wiley.com.]

particles. This is because particle nucleation under monomer-starved conditions leads to formation of a large number of small particles. This introduces a significant reduction in the rate of radical capture per particle and, therefore, in the kinetic regime of the polymerization reaction. As a result, the entry of second radicals becomes kinetically less important because most polymer particles containing a growing radical undergo chain transfer to monomer and radical exit before a second radical can enter the particle. Furthermore, radical termination in small particles, even though starved, are rather fast. With increasing [*S*] or decreasing R_a, the fraction of particles containing two or more growing radicals decreases and the polymerization system becomes more similar to microemulsion polymerization.

Figure 5 shows the model predictions for the population of particles at the mid of feeding for $R_a = 5.3 \times 10^{-6}$ l s^{-1} l^{-1} (aq) with $z = 3$. The size distribution of particles predicted with $z = 3$ is relatively broad, when compared with that of $z = 2$ (see Figure 3b). Note that $z = 3$ predicts a much smaller number of particles than $z = 2$. So particles undergo a more significant growth for the fixed quantity of the monomer added to the reactor. With z value of 3, most of the particles are inactive and only a small fraction of particles contains one growing radical; a real zero-one system. It may be inferred from Figure 5 that a broad size distribution of latexes may be a consequence of a depressed rate of radical entry and the associated stochastic broadening. We will test this hypothesis in the next section.

Evolution of PSD. It is often stated that semibatch emulsion polymerization produces broader size distribution than the batch polymerization. We have already shown that the PSD at the end nucleation becomes significantly sharper with decreasing rate of monomer addition. Therefore, the evolution of PSD during the growth stage cannot be easily decoupled from that in the nucleation stage. Such a difficulty

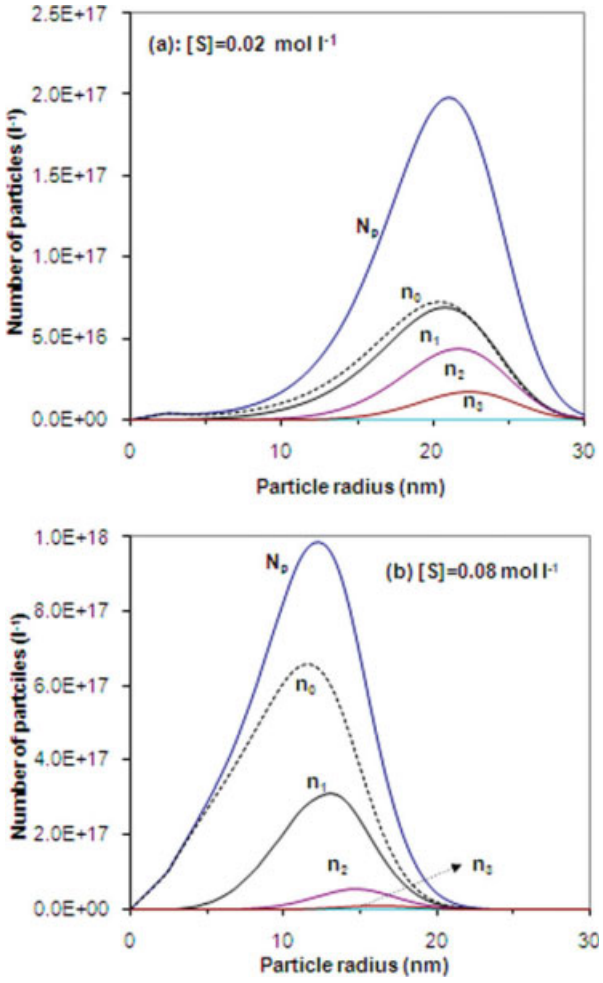

Figure 4. Size distributions for particles containing *n* radicals at the mid of feeding for two surfactant concentrations: (a) 0.02, (b) 0.08 mol l^{-1} (R_a = 2.6 × 10^{-5} l s^{-1} l^{-1} (aq), [*I*] = 2 × 10^{-3} mol l^{-1}, $t_{1/2}$ = 120 min, *z* = 2).

[Color figure can be viewed in the online issue, which is available at www.interscience.wiley.com.]

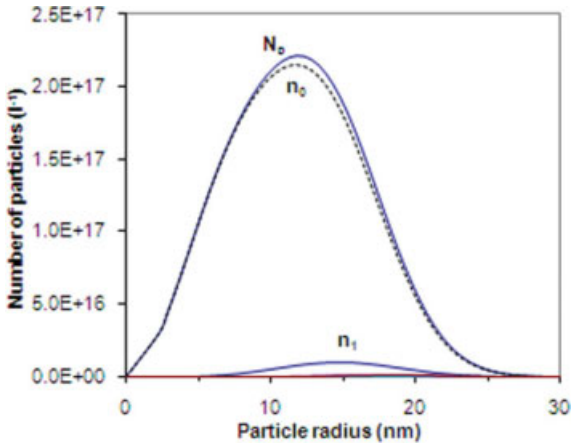

Figure 5. Size distributions for particles containing 0 or 1 radical at the mid of feeding for a typical run with $z = 3$.

See Figure 3b for comparison with $z = 2$ ($R_a = 5.3 \times 10^{-6}$ l s^{-1} l^{-1} (aq), $[S] = 0.04$ mol l^{-1}, $[I] = 2 \times 10^{-3}$ mol l^{-1}, $t_{1/2} = 120$ min). [Color figure can be viewed in the online issue, which is available at www.interscience.wiley.com.]

does not exist for the runs using different surfactant concentrations because their PSDs at the end of nucleation are similar, if not identical. Therefore, the evolution of PSDs during the growth stage can be independently studied.

Figure 6 shows the final PSDs predicted by zero-one and zero-one-two-three models for the runs using surfactant concentration of 0.02, 0.04, and 0.08 mol l^{-1}. The PSDs at the end of nucleation is also shown in the graph. It is clear from the graph that the size distribution of particles broadens with the surfactant concentration during the growth stage for both models. The major feature of a system with a low $\bar{n}$ ($<<0.5$) is that its PSD broadens with time, a phenomenon called stochastic broadening. This broadening occurs because growing particles outstrip nongrowing ones. The growing particles remain in the state of growth for a long time, so their size becomes quite large compared with that of the nongrowing particles. For a system with a low $\bar{n}$, the interchange between the growing and nongrowing particles is not fast and slows down with decreasing $\bar{n}$. A larger number of particles account for a lower rate of radical entry per particle and as a result a smaller $\bar{n}$. The broadest distribution was obtained for the highest surfactant concentration used (0.08 mol l^{-1}), as shown in Figure 6, which produced the largest number of particles. Figure 6 also shows that broadening is depressed to some extent if particles are bound to have either zero or one radical (zero-one model). The zero-one-two-three model predicts a broader distribution simply because particles with two or three radicals can grow at a higher rate. It is also inferred from the simulation results that zero-one-two-three assumption becomes more essential when either $[S]$ is small or R_a is high. With a low R_a or a high $[S]$, particle formation is significantly enhanced so that individual particles are confined to a zero-one system with a small fraction of particles containing a growing radical. Under such conditions, a zero-one model can adequately describe the kinetics of polymerization.

It should be noted that a PSD with a constant volumetric growth rate for particles usually narrows with reaction time when expressed in terms of radius. This self-sharpening effect is because a volumetric growth rate of particles is increasingly damped when it is expressed in terms of radius. It is clear from Figure 6 that the PSDs for all surfactant concentrations undergo a severe broadening during the growth stage despite simultaneous self-sharpening effect.

Comparison with experimental data

Experimental data on PSD in monomer-starved semibatch emulsion polymerizations are very rare. The model presented here is tested against the experimental PSD data available in the literature.[6,12] The semibatch emulsion polymerization reactions (70°C) were started by monomer being fed at a low rate to the reaction vessel containing deionized water, an emulsifier (sodium lauryl sulfate, SLS), and an initiator (potassium persulfate, KPS). A very small amount of monomer (1.78×10^{-3} mol l^{-1} (aq)) was also placed in the initial charge. Three set of experiments with [SLS], [KPS], and R_a as variables were carried out. The PSDs of the latexes at the mid of feeding ($t_{1/2}$) and end of polymerization (t_{final}), both after the completion of nucleation, were measured using transmission electron microscopy. After the end of feeding, 30 min were allowed for the finishing stage of polymerization (t_{final} (min) $= 2t_{1/2} + 30$). In this article, the size distribution data are presented in terms of radius. For the construction of the predicted PSDs, plots were made by conversion of the theoretical bin size (radius increment of 0.50 nm) to experimental ones (2.5 nm). The simulation results presented in the previous sections are also based on the experimental conditions described earlier but presented in terms of theoretical bin size (0.50 nm).

Before proceeding, it should be mentioned that it was not the intention of this article to find the best fit to the experimental data but to explain and analyze the evolution of PSD under starved conditions. In fact, a perfect data fitting cannot be aimed with the entry model used here because of lack of

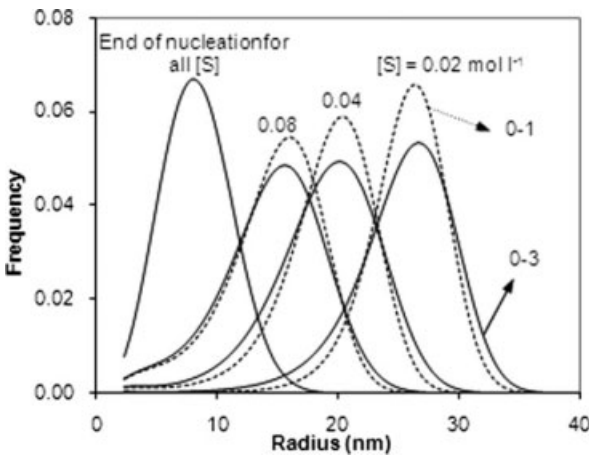

Figure 6. Final PSDs for various surfactant concentrations ($R_a = 2.6 \times 10^{-5}$ l s^{-1} l^{-1} (aq), $[I] = 2 \times 10^{-3}$ mol l^{-1}, $t_{final} = 240 + 30$ min, $z = 2$).

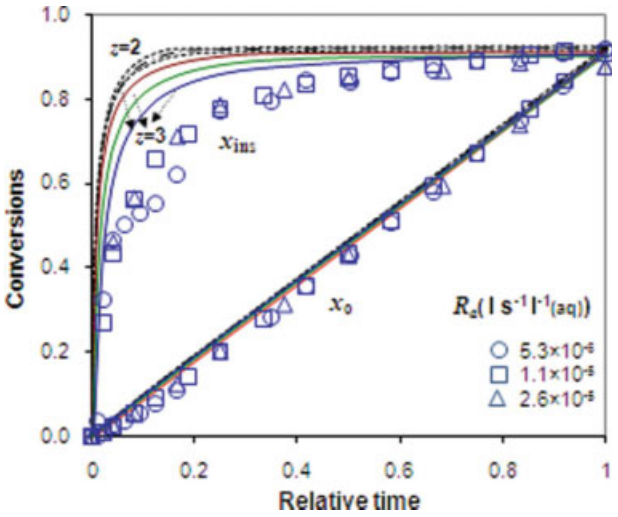

Figure 7. Predicted (lines) and experimental (symbols) instantaneous conversion (x_i) and overall conversion (x_o) in terms of relative time for runs with various rates of monomer addition and z values of 2 and 3 ([*I*] = 2 × 10^{-3} mol l^{-1}, [*S*] = 0.04 mol l^{-1}).

[Color figure can be viewed in the online issue, which is available at www.interscience.wiley.com.]

continuity in the model parameter z. The smallest possible change in z, from z value of 2 to 3 for example, introduces a significant variation in N_p that leaves little possibility for data fitting. As a result, poor agreement in some cases is due to the imperfections in the model predictions of other parameters. However, the model adopted here can satisfactorily show the trend of variations.

Rate of polymerization Typical results for the rate of polymerization in terms of relative time (i.e., time divided by the overall feeding time) have been shown in Figure 7 for various monomer feed rates and z values of 2 and 3. It is clear from the results that the polymerizations occurred under starved conditions right from the beginning. Generally, the model overpredicts the instantaneous conversion (x_i) in the early stage of the polymerizations. The inclusion of the routine for monomer solubilization in the micelles in the model improved model predictions of early conversion-time histories, but was unable to provide the exact fit. This overestimation, however, is thought to be due to the limitation in monomer transport from the added monomer droplets to the polymerising drops which was not taken care of by the model. The agreement between the experimental data and predictions, however, is better for $z = 3$.

The experimental conversions were almost insensitive to the rate of monomer addition in the later stage of polymerization (growth stage). This was congruent with the predicted conversions being practically insensitive to model assumptions including the critical chain length for entry (z = 2 or 3) and the number of radicals contained in the particles (0-1 or 0-1-2-3). This was expected because the rate of polymerization is tightly controlled by the rate of monomer addition under monomer-starved conditions.

Number of particles Figure 8 depicts the variation in the final number of polymer particles (N_p) with [S] and R_a, together with the model predictions. The model predictions with $z = 2$ are more consistent with the experimental data. The $N_p - R_a$ trend observed in Figure 8a can be explained as follows: At high R_a values, the rate of monomer addition is higher than the rate at which the monomer is polymerized in the particles ($R_p \ll R_a$). As a result monomer droplets form in the mixture and particles become saturated (flooded) with the monomer. For the same reason N_p is similar to that in the conventional batch emulsion polymerization and independent of R_a ($N_p \propto R_a^0$). As R_a further decreases, the regime of particle formation starts under monomer-flooded conditions (F), but later progresses to monomer-starved (S) conditions. Nucleation in this transition region is shown by (F-S) in Figure 8. Particle formation in this region is enhanced to an extent proportional to the length of the starved regime. With decreasing R_a, eventually a point is reached below which particle formation occurs exclusively under monomer-starved conditions. Model predictions indicate that the variations in N_p in terms of R_a corroborates with the analytical solution, $N_p \propto R_a^{-2/3}$, derived for polymerization of the styrenic type monomers under starved conditions. Similar explanation can be put forward for variations in N_p versus [S] (or [S]-[S]$_{CMC}$). A similar correlation to that predicted by the analytical model, $N_p \propto [S]^{1.0}$, is obtained

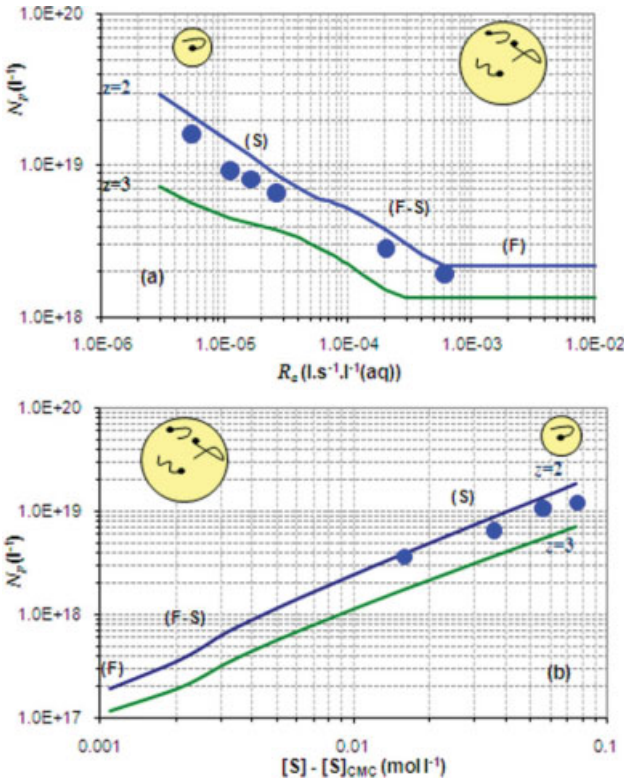

Figure 8. Variations in N_p versus (a) R_a and (b) [*S*] (conditions for (a): [*S*] = 0.04 mol l^{-1}, [*I*] = 2 × 10^{-3} mol l^{-1} and for (b): R_a = 2.6 × 10^{-5} l s^{-1} l^{-1} (aq), [*I*] = 2 × 10^{-3} mol l^{-1}).

[Color figure can be viewed in the online issue, which is available at www.interscience.wiley.com.]

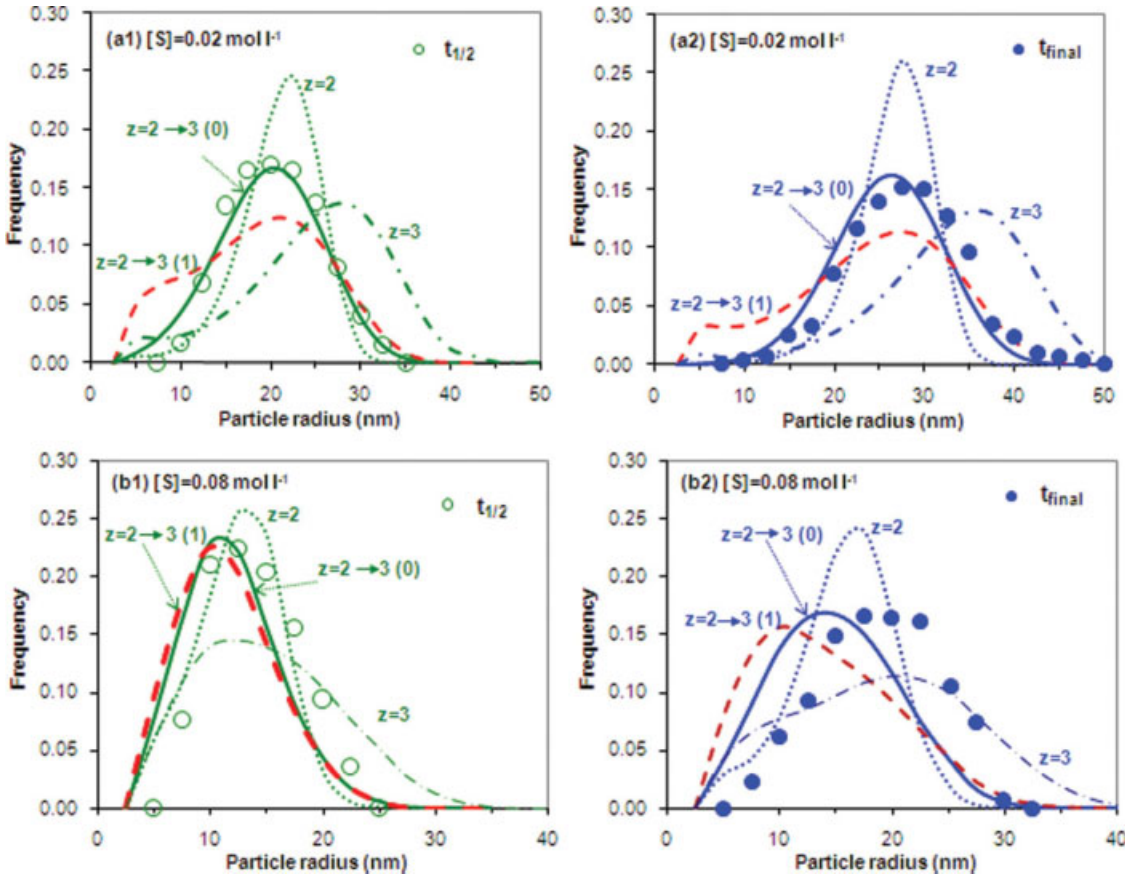

Figure 9. Experimental (symbols) and predicted (lines) PSDs using $z = 2$, $z = 3$, and two stage z models at the mid ($t_{1/2}$) and end of reactions (t_{final}) for runs with surfactant concentrations of (a) 0.02 and (b) 0.08 mol l^{-1}.

The model predictions for the two stage z model using $k_{ap} \propto r^1$ and $k_{ap} \propto r^0$ assumptions are shown by $z = 2 \rightarrow 3$ (1) and $z = 2 \rightarrow 3$ (0), respectively ($[I] = 2 \times 10^{-3}$ mol l^{-1}, $R_a = 2.6 \times 10^{-5}$ l s^{-1} l^{-1} (aq), $t_{1/2} = 120$ min, $t_{final} = 240 + 30$ min). [Color figure can be viewed in the online issue, which is available at www.interscience.wiley.com.]

for the starved regime from Figure 8b. As previously stated, the fraction of particles having more than one growing radical decreases with increasing $[S]$ or decreasing R_a and the polymerization system becomes more similar to microemulsion polymerization. The schematic presentation of such a trend is shown in Figure 8.

Particle size distribution The predicted PSDs at the mid ($t_{1/2}$) and end of polymerization (t_{final}) using z values of 2 and 3 are plotted in Figure 9 against the experimental data for the runs with the highest and lowest $[S]$ used. The final average diameter of particles formed with $[S] = 0.08$ mol l^{-1} is around 25 nm, which is comparable with those obtained from microemulsion polymerizations. Note that $[S] = 0.08$ mol l^{-1} is within the typical range of surfactant concentrations used in conventional emulsion polymerizations. This emphasizes that the kinetic similarity between microemulsion polymerization and monomer-starved semibatch emulsion polymerizations is established at a much lower surfactant concentration than what is usually used for a typical microemulsion polymerization.

It can be inferred from Figure 9 that the model prediction with $z = 2$ can give a good estimation of the average size of particles, but cannot account for the broadness observed in the experimental PSD. On the other hand, model predictions with $z = 3$ gave large particles but with a broad distribution comparable with the experimental PSD. Note that the poor agreement in case of $z = 3$ is partly due to the imperfections in the model prediction of the number of particles (different average sizes). It appears from the results that a z value between 2 and 3 can reproduce the data for the growth stage.

The PSDs predicted with $z = 2$ for $t_{1/2}$, which is rather close to the end of nucleation, are satisfactory for all $[S]$ in general and for $[S] = 0.08$ mol l^{-1} in particular, as seen in Figure 9. This results from the fact that a larger $[S]$ indicates a longer nucleation time. Therefore, the predicted PSD for $t_{1/2}$ for [S] = 0.08 mol l^{-1} is more representative of nucleation stage rather than growth stage. The extent of the broadening during the growth stage (from $t_{1/2}$ to t_{final}), however, is very severe and cannot be matched with the experiments. We have already shown in the modeling part that a significant PSD broadening occurs during the growth stage with $z = 2$. The reason for further broadening of the distributions is probably associated with the rate of radical entry into the polymer particles at high conversions. It should be pointed out that the decline in the rate of radical entry due to a

decrease in the concentration of growing radicals in the water phase at high conversions, owing to a low monomer concentration in the water phase, is already incorporated into the model. In addition, the variation in the rate of initiator decomposition with monomer concentration in the aqueous phase is very unlikely to be the main cause for the reduced rate of radical entry.

The entry of oligomeric radical into particles requires that first the hydrophobic part of the chain penetrates into polymer particles followed by propagation reaction of the radical therein so that it cannot be expelled from the particle. There is a lack of systematic studies of the surfactant self-assembly on hydrophobic solid surfaces. There seems to be an important difference between soft or solid hydrophobic interfaces.[36] On soft (fluid) surfaces, such as monomer-saturated particle/water interface, the hydrophobic chains are able to penetrate into the oil phase and keep out of the aqueous phase environment. This cannot happen on a solid interface and, as a result, the hydrocarbon chains cannot easily escape the aqueous phase environment. Polymers with a high T_g, such as polystyrene, may allow for a limited radical entry into polymer particles at high conversions because of the weaker adsorption. The similarity between the broadness of predicted (with $z = 3$) and experimental distributions suggests that the rate of entry into particles undergoes a substantial decline during the high-conversion polymerization. It is possible to define an efficiency function for radical entry in terms of free volume of polymer particles (or w_p), for example, that accounts for the decline in the entry rate at high conversions. We assume, however, that the lower radical flux at high conversions can be manifested by a unit rise in the critical chain length for entry; from $z = 2$ to $z = 3$ at the end of nucleation. This corresponds to the conditions whereby particles are either glassy or very close to their T_g. This assumption is conceptually pertinent because overall hydrophobic character of a surface active species grows with the length of its hydrophobic chain and as a result the thermodynamic driving force for adsorption becomes stronger as more of the molecules are adsorbed onto the polymer surface. This would probably increase the relaxation time of the radical on the surface of particles and thus increase the radical capture efficiency. The results for two-stage z model, $z = 2 \rightarrow 3$, as shown in Figure 9, can clearly reproduce the broadness observed in the experimental PSD. The assumption of unit jump in the critical length for radical entry at high conversions makes the simulation results more comparable with the experimental ones owing to the fact that N_ps predicted with $z = 2$ are close to the experimental values. This assumption is also consistent with the results shown in Figure 7 that indicate $z = 3$ can give a better prediction of the rate of polymerization during the growth stage.

An analysis was carried out on the skewness of PSDs. The experimental results indicate that while the PSDs are broad, they are more symmetric than skewed (or less skewed than the predicted PSDs). The PSD curves, obtained with the two-stage z model, reveal a strong degree of positive skewness. Although the stochastic broadening of the PSDs is associated with the zero-one nature of the system (i.e., an extremely low $\bar{n}$ as seen in Figure 5), the evolution of the skewness originates from uneven rate of radical entry into particles of different sizes. The extensive skewness predicted by the model occurs because the rate of radical entry into polymer particles was assumed to be proportional to the particle radius ($k_{ap} \propto r^1$). Furthermore, smaller particles have a lower monomer concentration and as a result they grow at a lower rate. To analysis the effect of radical entry in relation to the size of particles, we consider that the growth of the aqueous phase free radicals to a particular degree of polymerization, z, is the rate-determining step for free radicals captured by latex particles during the growth stage at high conversions; the rate of entry is independent of size and equal to $\rho_{entry} = k_{pw}^{z-1}[M]_w[I\dot{M}_{z-1}](N_P/N_A)$. This assumption, so called propagation-controlled entry, has been reported to fit several styrene emulsion polymerization systems with monodisperse seed particles.[28] The application of this hypothesis to polydisperse particles serves to evaluate the

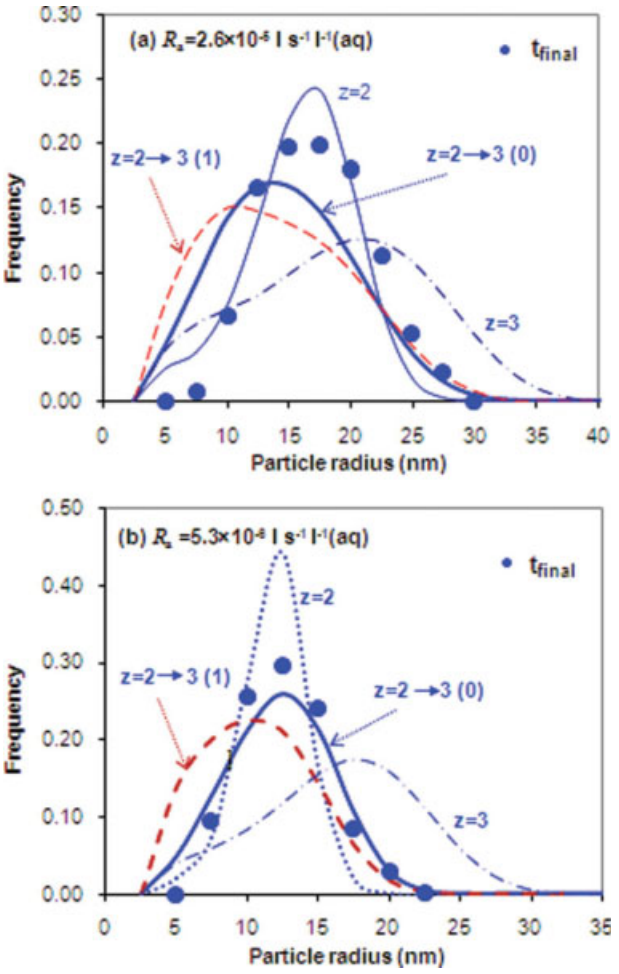

Figure 10. Experimental (symbols) and predicted (lines) PSDs at the end of reaction (t_{final}) for runs with monomer addition rates of 2.6 × 10^{-5} and (b) 5.3 × 10^{-6} l s^{-1} l^{-1} (aq) ([*I*] = 2 × 10^{-3} mol l^{-1}, [*S*] = 0.04 mol l^{-1}, t_{final} = 120 + 30 and 480 + 30 min for (a) and for (b), respectively).

See caption of Figure 9 for more details. [Color figure can be viewed in the online issue, which is available at www.interscience.wiley.com.]

effect of size-dependent entry coefficient on the skewness of the PSDs predicted at high conversions. Figure 9 clearly shows that the prediction of two-stage z model is improved if the rate of entry is assumed to be independent of the size of particles ($k_{ap} \propto r^0$).

Figure 10 illustrates the experimental and predicted PSDs at t_{final} for the runs with the lowest and highest monomer feed rates. Similar to the results for the surfactant series, the model predictions with $z = 2$ are narrower than the experimental ones, but those with $z = 3$ are much broader. The two-stage z model can give a better prediction of breadth of PSDs for both runs. One can conclude from the simulation results that the evolution of breadth of PSDs during the growth stage can be fairly well explained by a depressed rate of radical entry into the polymer particles.

Conclusion

Population balance modeling of a fully monomer-starved semibatch emulsion polymerization is reported for the first time. A 0-1-2-3 model was developed that covers a wide range of polymerization conditions encountered in semibatch emulsion polymerizations. Both 0-1 and pseudo-kinetics models fail to present very accurate predictions in the transition region. The model takes into account new features such as diffusion-controlled propagation during nucleation stage, as well as monomer partitioning into the micelles. The novel conclusions are:

(1) The PSDs, as well as the average particle size, at the end of nucleation in monomer-starved semibatch emulsion polymerization are independent of the surfactant concentration (the end of nucleation is marked by the disappearance of emulsifier micelles and not monomer).

(2) Monomer-starved nucleation can lead to formation of sharp PSDs. The PSDs at the end of nucleation become sharper with decreasing rate of monomer addition.

(3) A simple analytical equation has been derived (Eq. 51) which clearly indicates the average diameter of particles at the completion of nucleation is independent of surfactant concentration but varies with the rate of monomer addition.

(4) The breadth of distribution for a coagulation-free system with a single nucleation interval (no secondary nucleation) has been traditionally correlated with the nucleation time. It was shown here that a sharper PSD can be obtained at a longer nucleation time under monomer starved conditions.

(5) The broad PSD at the end of polymerization for monomer-starved semibatch emulsion polymerization is the results of stochastic broadening during the growth stage because of formation of a large number of particles.

(6) Only a small fraction of batch emulsion polymerizations usually occurs at very high conversions. As a result, any possible effect of variations in the rate of radical entry at high conversions on the PSD is minimum, and thus cannot be experimentally verified. For a fully monomer-starved semibatch process, whole polymerization occurs at high conversions. A theory was suggested to account for the reduced rate of radical entry at high conversions. Such an assumption was found to be essential for predicting the final PSDs, but not as equally important for the average size.

Literature Cited

1. Nomura M, Harada M. In: Basset DR, Hamielec AE, editors. *Emulsion Polymers and Emulsion Polymerization*. Chapter 6, *On the optimal reactor type and operation for continuous emulsions polymerization. ACS Symposium Ser* No 165, American Chemical Society 1981:121.
2. Chatterjee SP, Barnerjee M, Konar RS. Molecular-weight of polystyrene polymer obtained in the emulsion polymerization at low monomer concentration and the Harkins-Smith-Ewart-Gardon Theory. *J Polym Sci Polym Chem Ed*. 1979;17:2193–2207.
3. Sajjadi S, Brooks BW. Semibatch emulsion polymerization of butyl acrylate. I. Effect of monomer distribution. *J Appl Polym Sci*. 1999;74:3094–3110.
4. Gerrens H. On semicontinuous emulsion polymerization. *J Polym Sci Part C*. 1969;27:77–93.
5. Sajjadi S, Yianneskis M. Semibatch emulsion polymerization of methyl methacrylate with a neat monomer feed. *Polym React Eng*. 2003;11:715–736.
6. Sajjadi S. Particle formation under monomer starved conditions in the semibatch emulsion polymerization of styrene. I. Experimental. *J Polym Sci*. 2001;39:3940–3952.
7. Xu XJ, Chow PY, Quek CH, Hng HH, Gan LM. Nanoparticles of polystyrene latexes by semicontinuous microemulsion polymerization using mixed surfactants. *J Nanosci Nanotech*. 2003;3:235–240.
8. Ming WH, Jones FN, Fu SK. Synthesis of nanosize poly(methyl methacrylate) microlatexes with high polymer content by a modified microemulsion polymerization. *Polym Bull*. 1998;40:749–756.
9. Rabelero M, Zacarias M, Mendizabal E, Puig JE, Dominguez JM, Katime I. High-content polystyrene latex by microemulsion polymerization. *Polym Bull*. 1997;38:695–700.
10. Hermanson KD, Kaler EW. Kinetics and mechanism of the multiple addition microemulsion polymerization of hexyl methacrylate. *Macromolecules*. 2003;36:1836–1842.
11. He G, Pan Q, Rempel GL. Synthesis of poly(methyl methacrylate) nanosize particles by differential microemulsion polymerization. *Macromol Rapid Commun*. 2003;24:585–588.
12. Sajjadi S, Yianneskis M. Analysis of particle formation under monomer-starved conditions in emulsion polymerization reactors. *Macromol Symp*. 2004;206:201–213.
13. Zeaiter J, Romagnoli JA, Barton GW, Gomes VG, Hawkett BS, Gilbert RG. Operation of semi-batch emulsion polymerisation reactors: modelling, validation and effect of operating conditions. *Chem Eng Sci*. 2002;57:2955–2969.
14. Krackeler JJ, Naidus H. Particle size and molecular weight distributions of various polystyrene emulsions. *J Polym Sci Part C*. 1969;27:207–235.
15. Sajjadi S. Nanoparticle formation by monomer-starved semibatch emulsion polymerization. *Langmuir*. 2007;23:1018–1024.
16. Ledezma R, Trevino ME, Elizalde LE, Perez-Carrillo LA, Mendizabal E, Puig JE, Lopez RG. Semicontinuous heterophase polymerization under monomer starved conditions to prepare nanoparticles with narrow size distribution. *J Polym Sci Part A: Polym Chem Ed*. 2007;45:1463–1473.
17. Min KW, Ray WH. On the mathematical modeling of emulsion polymerization reactors. *J Macromol Sci Rev Macromol Chem Phys*. 1974;2:177–255.
18. Kiparissides C, Ponnuswamy SR. Application of population balance-equations to latex reactors. *Chem Eng Commun*. 1981;10:283–291.
19. Sundberg DC. Quantitative treatment of particle-size distributions in emulsion polymerization. *J Appl Polym Sci*. 1979;23:2197–2214.
20. Coen EM, Gilbert RG, Morrison BR, Leube H, Peach S. Modelling particle size distributions and secondary particle formation in emulsion polymerization. *Polymer*. 1998;39:7099–7112.
21. Araujo PHH, de la Cal JC, Asua JM, Pinto JC. Modeling particle size distribution (PSD) in emulsion copolymerization reactions in a continuous loop reactor. *Macromol Theory Simul*. 2001;10:769–779.
22. Crowley TJ. Meadows ES. Kostoulas E. Doyle FJ III. Control of particle size distribution described by a population balance model of semibatch emulsion polymerization. *J Process Control*. 2000;10:419–432.
23. Immanuel CD, Cordeiro CF, Sundaram SS, Doyle FJ III. Population balance PSD model for emulsion polymerization with steric stabilizers. *AIChE J*. 2003;49:1392–1404.

24. Vale HM, McKenna TF. Modeling particle size distribution in emulsion polymerization reactors. *Prog Polym Sci*. 2005;30:1019–1048.
25. Sajjadi S. Particle formation under monomer-starved condition in the semibatch emulsion polymerization of styrene. II. Mathematical modelling. *Polymer*. 2003;44:223–237.
26. Giannetti E. Nucleation mechanisms and particle-size distribution of polymer colloids. *AIChE J*. 1993;39:1210–1227.
27. Maxwell IA, Morrison BR, Napper DH, Gilbert RG. Entry of free radicals into latex particles in emulsion polymerization. *Macromolecules*. 1991;24:1629–1640.
28. Gilbert RG. *Emulsion Polymerization: A Mechanistic Approach*. London: Academic press, 1995.
29. Hansen FK, Ugelstad J. Particle formation in emulsion polymerization. I.Theory for homogeneous nucleation. *J Polym Sci Polym Chem Ed*. 1978;16:1953–1979.
30. Hansen FK, Ugelstad J. Particle formation in emulsion polymerization. III. Nucleation in systems with anionic emulsifier. *J Polym Sci Polym Chem Ed*. 1979;17:3047–3067.
31. Nomura M. In: Piirma I, editor. *Emulsion Polymerization*. Chapter 5, *Desorption and reabsorption of free radicals in emulsion polymerization*. New York: Academic Press, 1982:191–219.
32. Hawkett B, Napper DH, Gilbert RG. Analysis of interval III kinetic data for emulsion polymerizations. *J Chem Soc Faraday Trans*. 1981;77:2395–2404.
33. Soh S, Sundberg DC. Diffusion-controlled vinyl polymerization. III. Free volume parameters and diffusion-controlled propagation. *J Polym Sci: Polym Chem Ed*. 1982;20:1345–1371.
34. Martin,FL. Hamielec AE. High-conversion diffusion-controlled polymerization of styrene. I. *J Appl Polym Sci*. 1982;27:489–505.
35. Vanzo EH, Marchess RH, Stannett V. Solubility and swelling of latex particles. *J Colloid Sci*. 1965;20:62.
36. Kumar N, Tilton RD. Unified model to predict self-assembly of surfactants in solution and adsorption on solid or fluid hydrophobic surfaces: effect of molecular structure. *Langmuir*. 2004;20:4452–4464.

Manuscript received Apr. 27, 2008, and revision received Mar. 6, 2009.